ACADEMIC PRESS

Available online at www.sciencedirect.com

SCIENCE DIRECT®

Journal of Magnetic Resonance 158 (2002) 23–35

JMR Journal of Magnetic Resonance

www.academicpress.com

A 2D MAS solid-state NMR method to recover the amplified heteronuclear dipolar and chemical shift anisotropic interactions

Yufeng Wei,[a,1] Dong-Kuk Lee,[a] Ann E. McDermott,[b] and A. Ramamoorthy[a,*]

[a] *Department of Chemistry and Biophysics Research Division and Department of Macromolecular Science and Engineering, The University of Michigan, Ann Arbor, MI 48109, USA*

[b] *Department of Chemistry, Columbia University, New York, NY 10027, USA*

Received 7 December 2001; revised 20 June 2002

Abstract

A two-dimensional solid-state NMR method for the measurement of chemical shift anisotropy tensors of X nuclei (^{15}N or ^{13}C) from multiple sites of a polypeptide powder sample is presented. This method employs rotor-synchronized π pulses to amplify the magnitude of the inhomogeneous X–CSA and ^{1}H–X dipolar coupling interactions. A combination of on-resonance and magic angle rf irradiation of protons is used to vary the ratio of the magnitudes of the ^{1}H–X dipolar and X–CSA interactions which are recovered under MAS, in addition to suppressing the ^{1}H–^{1}H dipolar interactions. The increased number of spinning sidebands in the recovered anisotropic interactions is useful to determine the CSA tensors accurately. The performance of this method is examined for powder samples of *N*-acetyl-^{15}N-L-valine (NAV), *N*-acetyl-^{15}N-L-valyl-^{15}N-L-leucine (NAVL), and α-^{13}C-L-leucine. The sources of experimental errors in the measurement of CSA tensors and the application of the pulse sequences under high-field fast MAS operations are discussed.

Keywords: CSA; Dipolar coupling; MAS; Sideband enhancement; Multiple pulse sequence; Polypeptide

1. Introduction

Solid-state NMR techniques have been highly valuable in determining accurate chemical shift anisotropy (CSA) tensors, which are essential in the structural studies of peptides and proteins [1,2]. Recent studies suggest that the CSA tensor values and orientations of ^{15}N or ^{13}C nuclei present in the backbones of proteins depend on the primary and secondary structure, dynamics, and electrostatic effects [3–6]. Therefore, it is of significant interest to accurately determine the CSA tensors using solid-state NMR techniques. However, some of the intrinsic difficulties in using solid-state NMR spectroscopy, such as poor sensitivity and resolution, restrict the measurement of CSA tensors from proteins that are uniformly or nonselectively labeled with ^{15}N and/or ^{13}C isotopes [7,8]. In addition, in order to avoid the rotational resonance condition that recovers ^{13}C–^{13}C dipolar coupling [9], not all spinning speeds can be used to perform MAS experiments on uniformly ^{13}C-labeled proteins. Only selected spinning speeds are available: 50, 80–100, and 180 ppm or faster. The spinning speeds are expressed in ppm units to be magnetic-field-independent and to easily compare with a conventional 1D ^{13}C spectrum of a protein. Therefore, CSA tensors from a protein have to be measured at a relatively high spinning speed (>5 kHz at 400 MHz). On the other hand, the spans of CSA tensors associated with $^{13}C_{\alpha}$ and other ^{13}C nuclei present in the side chains of a protein are smaller than 50 ppm [3,7,10], and therefore a spinning speed >50 ppm is not desirable to measure such small CSA tensors. Therefore, it is essential to develop a new solid-state NMR method that can be used to measure small CSA tensors without sacrificing the high sensitivity and high resolution rendered by relatively fast spinning speeds, where conventional methods cannot be used to measure CSA and heteronuclear dipolar coupling.

* Corresponding author. Fax: 1-734-764-8776.
E-mail address: ramamoor@umich.edu (A. Ramamoorthy).
[1] Present address: Laboratory of Molecular Biophysics, Rockefeller University, 1230 York Avenue, New York, NY 10021, USA.

1090-7807/02/$ - see front matter
PII: S1090-7807(02)00056-3

To overcome the above-mentioned difficulties, we propose a simple two-dimensional solid-state NMR method that can be used to accurately determine the principal values and directions of the principal elements of the CSA tensors directly from polypeptides that are uniformly, or nonselectively, labeled with ^{15}N or ^{13}C isotopes. Based on the extended chemical-shift modulation method [11] and the amplification of dipolar coupling method [12], the proposed two-dimensional pulse sequences under MAS correlate the isotropic chemical shift of X nuclei (^{15}N or ^{13}C) and the convoluted X–CSA and ^{1}H–X dipolar coupling interactions. Rotor-synchronized π pulses in the X-rf channel are applied to amplify the magnitudes of X–CSA and ^{1}H–X dipolar coupling interactions, while a multiple pulse sequence is applied to suppress the ^{1}H–^{1}H dipolar interactions. Applying the ^{1}H–^{1}H dipolar decoupling sequence during part of the evolution time can further modulate the magnitude of the ^{1}H–X dipolar coupling. This method, essentially a simplified version of the extended chemical shift method [11], intentionally mixes dipolar coupling and CSA interactions in order to extract the angles between the two spin interaction tensors, which are important in studying protein structures and dynamics [3,13]. In recent years, several methods have been introduced to generate spinning sidebands in the indirect dimension by the use of π pulse timing within a rotor period. Besides the aforesaid extended chemical-shift modulation and amplification of dipolar coupling methods, which are based on separation of local field, Spiess and co-workers proposed a rotor encoding of longitudinal magnetization experiment to generate informative spinning sidebands in the indirect dimension [14]; Levitt and co-workers developed symmetry-based R- and C-type pulse sequences to selectively recouple heteronuclear dipolar couplings [15–17]. As in other studies, our method represents an additional useful way to manipulate spinning sidebands in the indirect dimension to obtain valuable information. The performance of this method is demonstrated on powder samples of *N*-acetyl-^{15}N-L-valine (NAV), *N*-acetyl-^{15}N-L-valyl-^{15}N-L-leucine (NAVL), and $^{13}C_{\alpha}$-L-leucine. The effects of rf power strength for the π pulse, errors in the π pulse length (or rf field inhomogeneity), and the offset (the frequency difference between the isotropic chemical shift of X nuclei and the rf irradiation) on the efficacy of the two-dimensional pulse sequence were also examined, using a numerical simulation program.

2. Theory

In an unperturbed (or rf-free) rotor period of MAS, the dynamic phase Φ accumulated by the nuclear spin magnetization due to the evolution under the effect of inhomogeneous CSA and heteronuclear dipolar coupling interactions is averaged out to zero [18]. On the other hand, when a π pulse is introduced after a time interval t_1 within a rotor period, as shown in Fig. 1A, the dynamic phase accumulated by the transverse magnetization of X nuclei (^{13}C or ^{15}N), due to the evolution under CSA and/or heteronuclear dipolar coupling interactions, at the end of a rotor cycle is given as [12]

$$\Phi(\tau_r) = \int_0^{t_1} \omega(t)\,\mathrm{d}t - \int_{t_1}^{\tau_r} \omega(t)\,\mathrm{d}t = 2\Phi(t_1). \quad (1)$$

It is clear that in the presence of a π pulse, the accumulated dynamic phase is no longer averaged to zero after a rotor period; in addition, at the end of a rotor period, the π pulse doubles the dynamic phase accumulated at time t_1. This doubling of the dynamic phase is equivalent to doubling the magnitude of the inhomogeneous interaction for a given spinning speed ω_r. Alternatively, if the magnitude of the inhomogeneous interaction is fixed then doubling the phase is equivalent to halving the spinning speed [12]. In general, if n rotor periods are used to repeat the basic scheme shown in Fig. 1A then the dynamic phase accumulated will be increased by $2n$ as given below:

$$\Phi(n\tau_r) = n\left(\int_0^{t_1} \omega(t)\,\mathrm{d}t - \int_{t_1}^{\tau_r} \omega(t)\,\mathrm{d}t\right) = 2n\Phi(t_1). \quad (2)$$

This idea is employed to design a two-dimensional rf pulse sequence (shown in Figs. 1B and C) that recovers the CSA of X nuclei as well as the ^{1}H–X heteronuclear dipolar coupling under MAS condition. In the pulse sequence given in Fig. 1B, the transverse magnetization of X nuclei prepared via cross-polarization (CP) from the ^{1}H magnetization is allowed to evolve under the CSA and the ^{1}H–X dipolar coupling for two rotor periods, and then the free induction decay is acquired under on-resonance proton decoupling. A π pulse after a time interval t_1 in each rotor period is used to amplify the phase accumulated by the X magnetization, while the π pulse at the end of the first rotor period ensures that the phase accumulated during each rotor period is identical and additive. Therefore, the phase accumulated by the transverse magnetization of X nuclei after the two complete rotor periods is quadrupled, which is equivalent to an effective fourfold reduction in the spinning speed, as explained earlier in this paper. Magic angle rf decoupling or the Lee–Goldburg (LG) decoupling sequence [19–21] is applied in the ^{1}H rf channel to suppress ^{1}H–^{1}H dipolar interactions for the two rotor periods, while the transverse magnetization of X nuclei evolves under the X–CSA and the scaled ^{1}H–X dipolar coupling interactions. The TPPM decoupling of protons is used during the acquisition of X magnetization [22]. Thus the two-dimensional spectrum obtained using this pulse sequence consists of isotropic chemical shifts of X nuclei in ω_2 and the convoluted X–CSA and ^{1}H–X dipolar coupling interactions in ω_1. Both the X–CSA

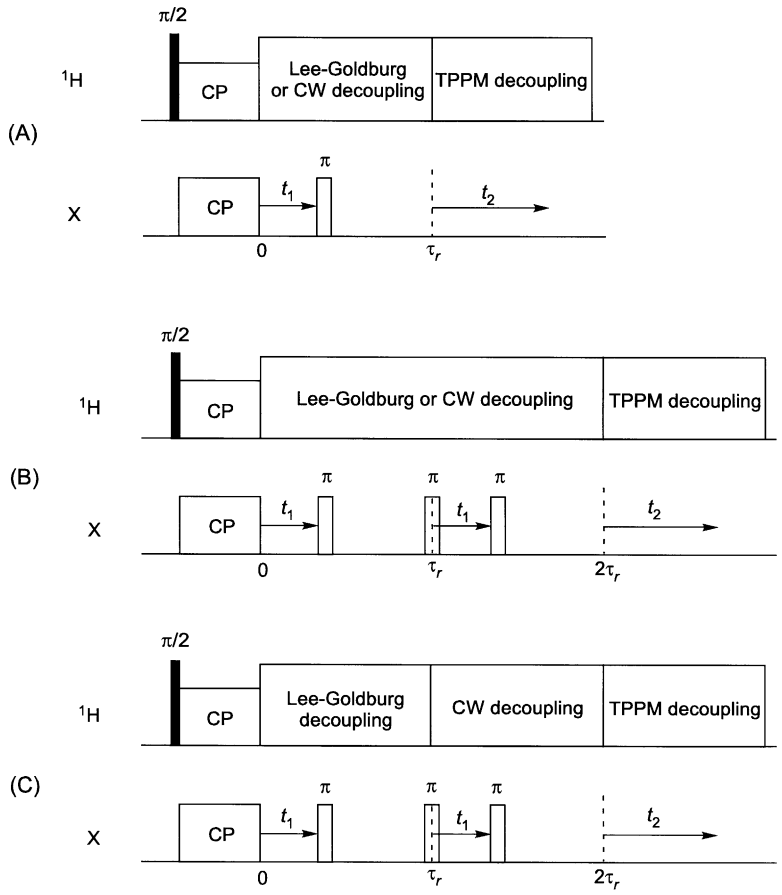

Fig. 1. Two-dimensional pulse sequences that recover inhomogeneous interactions, such as ^{1}H–X heteronuclear dipolar coupling and X–CSA, under MAS. (A) A basic one-rotor-cycle pulse sequence that recovers and doubles the magnitude of an inhomogeneous interaction. (B) A two-rotor-cycles pulse sequence that recovers and quadruples the magnitude of an inhomogeneous interaction. (C) A two-rotor-cycles pulse sequence that doubles the ^{1}H–X heteronuclear dipolar coupling while it quadruples the X–CSA interaction.

and ^{1}H–X dipolar coupling interactions are quadrupled, whereas the LG decoupling scales the ^{1}H–X dipolar coupling by 0.58. When a higher spinning speed is desired, more rotor periods can be used to further reduce the effective spinning speed in order to obtain more spinning sidebands in the ω_1 dimension of the 2D spectrum. The main limitation of this experiment is the finite π pulse length that restricts the attainable spectral width in the indirect frequency dimension of the 2D spectrum.

The LG decoupling can also be applied during one of the two rotor periods as illustrated in Fig. 1C. This pulse sequence would allow the ^{1}H–X dipolar coupling to be effective for one of the two rotor periods, while the CSA interaction would be effective for both rotor periods. Therefore, in this case, the CSA interaction is quadrupled, whereas the heteronuclear dipolar coupling is only doubled. If the spinning speed is still considered as a fourfold reduction then the magnitude of the CSA interaction remains the same as in the case of the pulse sequence in Fig. 1B, while the magnitude of the effective ^{1}H–X dipolar coupling is only half of the original, besides the scaling factor from the multiple pulse sequence. This partial-LG decoupling scheme (see Fig. 1C) is useful to measure the sideband pattern of the convoluted heteronuclear dipolar and CSA interactions, especially when the dipolar coupling is too large compared to the span of the CSA tensor; for example, the $^{13}C_{\alpha}$ CSA span is less than 2.0 kHz (at 9.4 T magnetic field) and the ^{1}H–$^{13}C_{\alpha}$ dipolar coupling is $\sim$20 kHz. It should be noted that the pulse sequences given in Fig. 1 are not intended to suppress the CSA interaction, while pulse sequences that completely suppress the CSA interaction in order to measure the heteronuclear dipolar interactions have already been reported in the literature [12,23,24].

3. Experimental

All of the experiments were performed on a Chemagnetics/Varian CMX Infinity-400 solid-state NMR spectrometer, operating at 40.551 MHz for ^{15}N, 100.620 MHz for ^{13}C, and 400.139 MHz for ^{1}H.

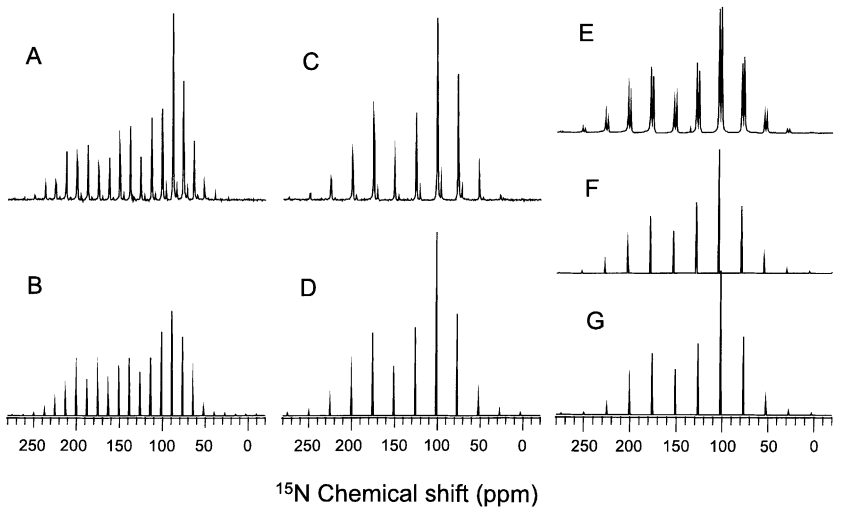

Fig. 2. Comparison of one-dimensional ^{15}N CSA spectral slices obtained from two-dimensional experiments on NAV and NAVL samples with one-dimensional CPMAS spectra. Two-dimensional spectra (not shown) were obtained using the pulse sequence given in Fig. 1B with an on-resonance continuous wave ^{1}H-decoupling during the t_1 period. (A) and (C) One-dimensional CPMAS spectrum of NAV sample at 500 Hz and 1 kHz spinning speed, respectively. (B) and (D) One-dimensional spectral slices obtained from 2D experiments on NAV sample at 2 and 4 kHz spinning speed, respectively. (E) 1D CPMAS spectrum of NAVL sample at 1 kHz spinning speed. (F) and (G) 1D spectral slices of leucine and valine residues, respectively, obtained from a 2D experiment on NAVL sample at 4 kHz spinning speed.

Conventional 5-mm rotors were used and 50 mg of ^{13}C- or ^{15}N-labeled samples were packed into the rotors. ^{1}H, ^{13}C, and ^{15}N 90° pulse lengths were optimized to 3.0, 3.7, and 4.4 μs, respectively. A contact time of 1.5 ms for CP, an acquisition time of 40 ms, and a recycle delay of 3 s were used for all samples. The TPPM decoupling of protons [13] was used during signal acquisition with a pulse duration of 5.67 μs and a total phase shift of 15°.

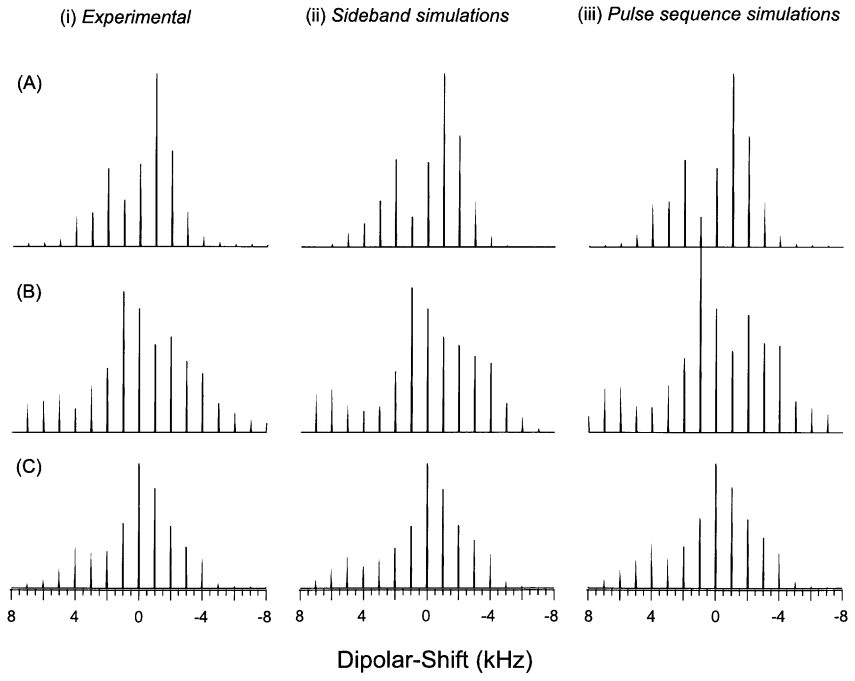

Fig. 3. One-dimensional spinning sideband patterns obtained from the 2D spectra (not shown) obtained from a powder sample of *N*-acetyl-^{15}N-L-valine (NAV) using the pulse sequences in Fig. 1 at 4 kHz MAS. (ii) The best-fitting simulated spectra and (iii) numerically simulated spectra obtained as explained in the text. (A) CSA spinning sideband patterns; (B) spinning sideband patterns of dipolar-shift interactions with two rotor periods of dipolar coupling evolution; (C) spinning sideband patterns of dipolar-shift interactions with one rotor period of dipolar coupling evolution. The simulated spectra were obtained using the following principal values of the ^{15}N CSA tensor: $\sigma_{11N} = 59.6$ ppm, $\sigma_{22N} = 89.4$ ppm, $\sigma_{33N} = 228.6$ ppm. The (α_N, β_N) angles used in simulated dipolar-shift spectra were (51°, 20°) in (B) and (36°, 16°) in (C). An N–H bond length of 1.07 Å and a spinning speed of 1 kHz were used in the simulations.

Table 1
$^{15}N/^{13}C$ CSA tensor values and angles in selected compounds

	σ_{iso} (ppm)	σ_{11} (ppm)	σ_{22} (ppm)	σ_{33} (ppm)	α (°)	β (°)
^{15}N-NAV						
1D (1 kHz)	125.9	58.0	83.0	236.6		
2D (4 kHz, no dipolar)	125.9	59.6	89.4	228.6		
2D (4 kHz, full dipolar)					51 ± 15	20 ± 1
2D (4 kHz, half dipolar)					36 ± 15	16 ± 2
1D (500 Hz)	125.9	61.2	83.1	233.2		
2D (2 kHz, no dipolar)	125.9	55.9	94.0	227.7		
2D (2 kHz, full dipolar)					36 ± 8	20 ± 2
2D (2 kHz, half dipolar)					32 ± 10	18 ± 2
2D MAT 200 Hz[a]	125.5	59.6	80.5	235.3	20 ± 15	21 ± 2
^{15}N-NAVL Leucine						
1D (500 Hz)	128.3	57.5	93.3	234.1		
1D (1 kHz)	128.3	54.7	98.3	231.8		
2D (4 kHz, no dipolar)	128.3	56.6	102.9	225.4		
2D(4 kHz, full dipolar)					48 ± 15	16 ± 2
2D (4 kHz, half dipolar)					36 ± 20	15 ± 2
2D MAT 200 Hz[a]	128.4	58.7	93.7	232.8	36 ± 11	18 ± 2
2D MAT 500 Hz[a]	128.4	58.7	93.7	232.8	41 ± 11	17 ± 3
^{15}N-NAVL Valine						
1D (500 Hz)	125.9	58.2	87.1	232.2		
1D (1 kHz)	125.9	57.2	88.6	231.8		
2D (4 kHz, no dipolar)	125.9	57.3	93.9	226.5		
2D (4 kHz, full dipolar)					54 ± 20	17 ± 2
2D (4 kHz, half dipolar)					27 ± 25	16 ± 2
2D MAT 200 Hz[a]	125.7	60.2	87.1	230.1	34 ± 12	20 ± 2
2D MAT 500 Hz[a]	125.7	60.2	87.1	230.1	44 ± 13	19 ± 2
^{13} C_α-L-Leucine						
Site 1, 2D, 8 kHz	54.4	43.8	56.1	63.3	0 ± 20	90 ± 5
Site 2, 2D, 8 kHz	53.4	43.0	55.4	61.9	0 ± 20	90 ± 5
L-Leucine[b]	54.4	42	42	80		
	53.2	40	40	80		
L-Alanine single crystal[c]	50.9	31.2	56.4	65.0		
L-Threonine single crystal[d]	60.2	52.6	58.9	69.0		

[a] Reference [8].
[b] Reference [30].
[c] Reference [31].
[d] Reference [32].

From 64 to 128 transients were accumulated for each t_1 increment. MAS speeds of 2000 ± 1 and 4000 ± 1 Hz were used in ^{15}N experiments and 8000 ± 1 Hz for ^{13}C experiments. Two rotor periods for ^{15}N experiments and four rotor periods for ^{13}C experiments were used for the dipolar-shift evolution. The LG ^{1}H–^{1}H dipolar decoupling condition was obtained by offsetting the ^{1}H rf irradiation frequency by 59,924 Hz. Three types of evolution in the t_1 period of the pulse sequence in Fig. 1 were employed: (a) CW proton decoupling during all the rotor periods, allowing only the CSA interaction to be effective; (b) LG decoupling during all the rotor periods, allowing the scaled ^{1}H–X dipolar and the complete X–CSA interactions to be effective; (c) LG decoupling during part of the rotor periods and CW proton decoupling during the remaining rotor periods, leaving the partial dipolar and complete CSA interactions operative. A π pulse was moving from 0 to τ_r within a rotor period in 32 steps (or 32 t_1 increments) for experiments at 2 kHz MAS, and 16 steps (or 16 t_1 increments) for experiments at 4 kHz MAS, with a t_1 dwell time of 15.6 μs in ^{15}N experiments. In ^{13}C experiments, 16 t_1 increments were used under 8 kHz MAS, with a t_1 dwell time of 7.8 μs. All experiments were performed by setting the individual resonance peak on resonance in order to remove any additional phase acquired by the X magnetization due to the evolution under the isotropic chemical shift of X nuclei.

The one-dimensional dipolar-shift sideband patterns obtained from the ω_1 frequency dimension of the 2D spectrum were compared with the simulated spectra. The simulated spectra were obtained using a C++ program, compiled under a GAMMA-4.0.3β developmental environment [25] (http://gamma.magnet.fsu.edu/index.html) on a Silicon Graphics (Octane) workstation and also on an AMD K6-II PC. The root-mean-square

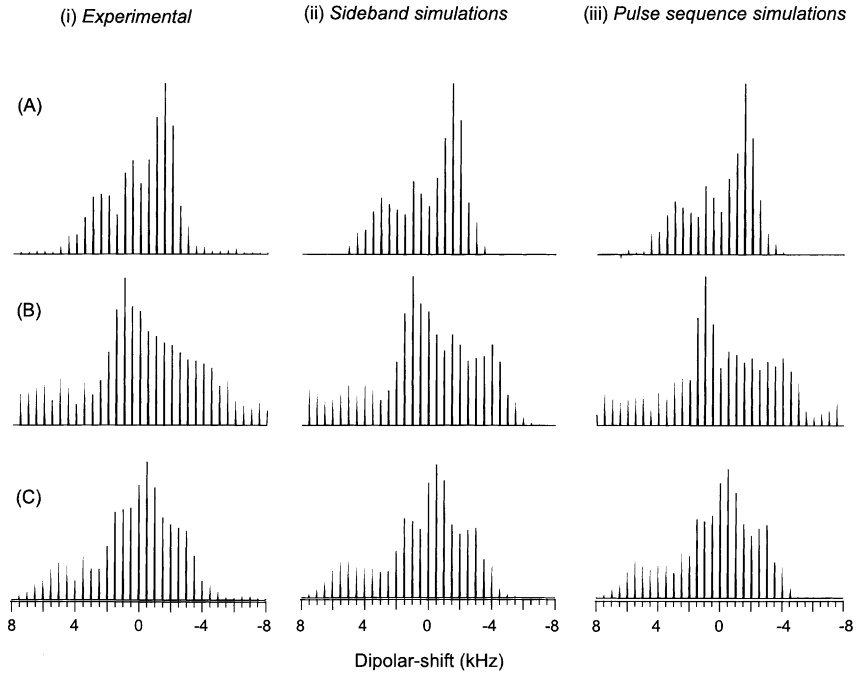

Fig. 4. (i) One-dimensional spinning sideband patterns obtained from the 2D spectra (not shown) obtained from a powder sample of *N*-acetyl-^{15}N-L-valine (NAV) using the pulse sequences in Fig. 1 at 2 kHz MAS. The best-fitting simulated spectra are shown in column (ii). The spectra from numerical pulse sequence simulations using the SIMPSON program are shown in column (iii). (A) Spinning sideband patterns of ^{15}N CSA; (B) spinning sideband patterns of dipolar-shift interactions with two rotor periods of dipolar coupling evolution; (C) spinning sideband patterns of dipolar-shift interactions with one rotor period of dipolar coupling evolution. The simulated spectra were obtained using the following principal values of the ^{15}N CSA tensor: $\sigma_{11N} = 55.9$ ppm, $\sigma_{22N} = 94.0$ ppm, $\sigma_{33N} = 227.7$ ppm. The (α_N, β_N) angles used in simulated dipolar-shift spectra were (36°, 20°) in (B) and (32°, 18°) in (C). An N–H bond length of 1.07 Å and a spinning speed of 0.5 kHz were used in the simulations.

deviations (RMSD) between the experimental and the simulated spectra were also calculated using the same program.

The pulse sequence was also numerically simulated using a simulation program, SIMPON [26] (http://nmr.imsb.au.dk). The effects of the strength of rf power for the π pulse, errors in the π pulse length (or rf field inhomogeneity), and the offset (the frequency difference between the isotropic chemical shift of X nuclei and the rf irradiation) on the efficacy of the 2D pulse sequences in Fig. 1 were also examined using this numerical simulation program.

4. Results and discussion

The magnitudes of the principal elements (defined as $\sigma_{33N} \geqslant \sigma_{22N} \geqslant \sigma_{11N}$) of the ^{15}N CSA tensors of NAV and NAVL peptides were obtained by one-dimensional CPMAS spectroscopy at 500-Hz and 1-kHz spinning speeds (Figs. 2A, C, and E), and the spinning sidebands were simulated using the Herzfeld and Berger method [27] and fitted computationally [28]. The principal values given in Table 1 are in agreement with the results obtained from 2D MAT experiments on the same samples [8].

The one-dimensional spectral slices can be obtained from the 2D spectra along the ω_1 frequency dimension. The high-resolution spectra were obtained by replicating t_1 FID and appending the replicated FID to the original data several times until the desired peak separation was achieved. Since CSA and/or dipolar coupling interactions form rotor echoes in FID and the magnetization is identical at the beginning and the end of the t_1 evolution period, FID replication is an effective way to obtain (pseudo) high resolution while keeping the experimental time short. Here, we replicated the 16- or 32-point FID to 512 points. No zero-filling was done to this FID as it introduced undesired spikes in the Fourier transformed spectrum (as seen in [12]). Since only the sideband intensity information is contained in the FIDs in t_1 dimension, zero filling and/or a weighing function introduce artificial linewidths, which are not present in the FIDs. Further, all the spinning sidebands in the ω_2 dimension should be summed together with the centerband. The experimental one-dimensional CSA-only spectral slices obtained from 2-D spectra of NAV and NAVL samples are shown in Figs. 2B and D for NAV and Figs. 2F and G for NAVL, in comparison with direct one-dimensional CPMAS spectra shown in Figs. 2A and C for NAV and Fig. 2E for NAVL. The CSA tensor values obtained from the computer simulation of

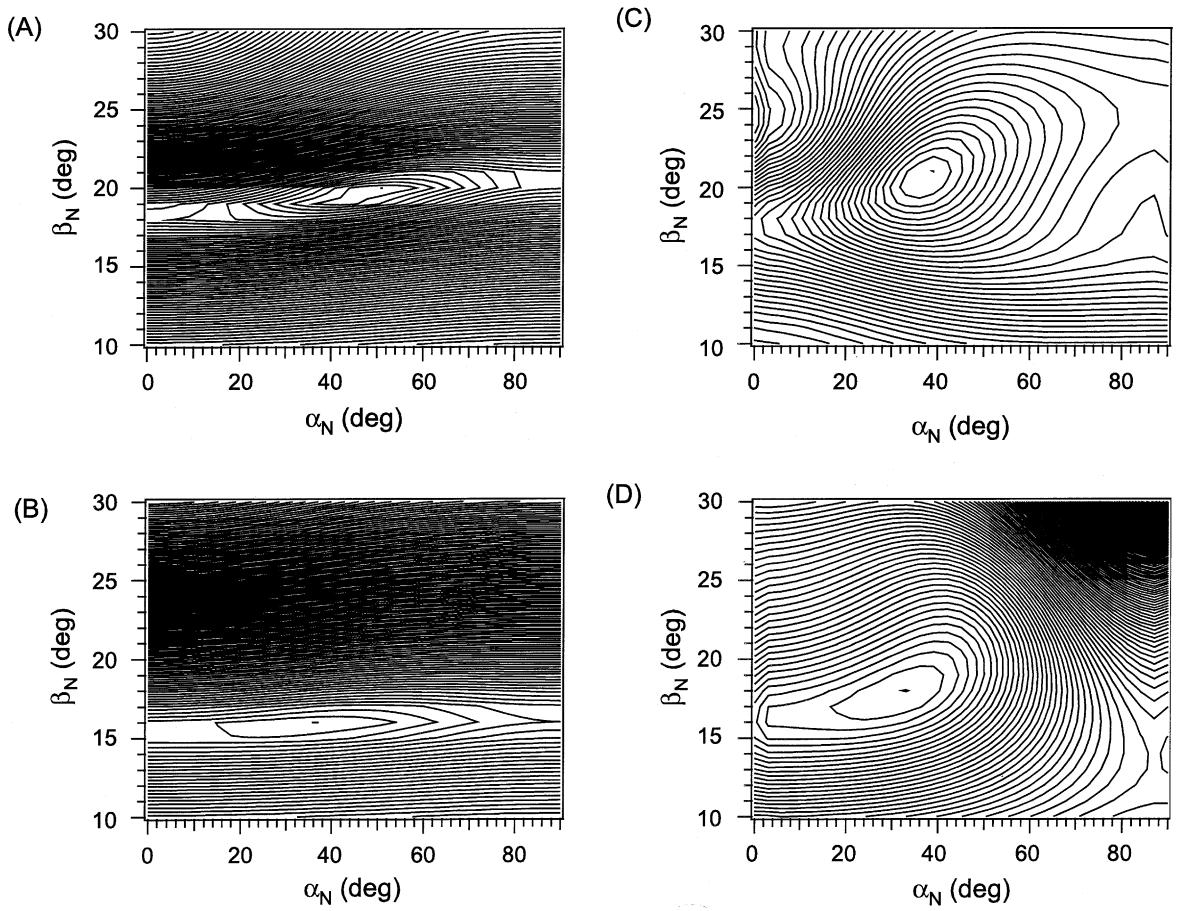

Fig. 5. Two-dimensional RMSD contour plots of simulated and experimental spectra of dipolar-shift experiments. The contour intervals are 10% of the minimum RMSD value. (A) An RMSD plot for the dipolar-shift experiment with two rotor periods of dipolar coupling evolution at 4 kHz MAS; the errors in the angles (α_N, β_N) estimated at the 10% RMSD level are (±15°, ±1°). (B) An RMSD plot for the dipolar-shift experiment with one rotor period of dipolar coupling evolution at 4 kHz MAS; the errors in the angles (α_N, β_N) estimated at the 10% RMSD level are (±15°, ±2°). (C) An RMSD plot for the dipolar-shift experiment with two rotor periods of dipolar coupling evolution at 2 kHz MAS; the errors in the angles (α_N, β_N) estimated at the 10% RMSD level are (±8°, ±2°). (D) An RMSD plot for the dipolar-shift experiment with one rotor period of dipolar coupling evolution at 2 kHz MAS; the errors in the angles (α_N, β_N) estimated at the 10% RMSD level are (±10°, ±2°).

the slices are also listed in Table 1. For both samples, the CSA principal values obtained from two-dimensional experiments are in good agreement with those obtained using 1D CPMAS experiments.

The experimental one-dimensional spectral slices of NAV sample obtained from 2D spectra at 4 and 2 kHz are given in Figs. 3 and 4 (column i), respectively. The sideband simulations using our program (column ii) and the numerical pulse sequence simulations using SIMPSON (column iii) are also presented in Figs. 3 and 4. The spinning sidebands are separated by 1000 Hz in Fig. 3 and 500 Hz in Fig. 4, confirming that the pulse sequences in Fig. 1 are successful in increasing the number of spinning sidebands by a factor of 4. Figs. 3A-i and 4A-i show the spectra obtained with the CW proton decoupling in both the rotor periods in t_1, in which only the CSA interaction is preserved. The spectra shown in Figs. 3A-ii and 4A-ii are best-fit spectra and the principal CSA tensor values are listed in Table 1. The spectra in Figs. 3A-iii and 4A-iii were numerically computed using the SIMPSON program by considering the ^{15}N–CSA and ^{1}H–^{15}N dipolar coupling interactions for a two spin-1/2 system with no additional protons. In addition, parameters used in the simulations were an isotropic chemical shift of zero (on resonance), an N–H dipolar coupling of 9.7 kHz (calculated using a N–H bond length of 1.07 Å), and on-resonance CW proton decoupling during both the rotor periods.

Figs. 3B-i and 4B-i show the spectra obtained with LG decoupling in both the rotor periods in t_1 (see Fig. 1B). The amplified ^{1}H–^{15}N dipolar coupling is scaled only by the LG decoupling with a scaling factor of 0.58. The angles α_N (the angle between the projection of the N–H bond on the σ_{11N}–σ_{22N} plane and the σ_{11N} axis) and β_N (the angle between the N–H bond and the σ_{33N} axis) define the orientation of the ^{15}N CSA tensors relative to the N–H bond [2]. The (α_N, β_N) angles used in the simulations of the best-fitting spectra are (51°, 20°) in Fig. 3B-ii and (36°, 20°) in 4B-ii. An N–H bond length of 1.07 Å was used in the simulations. The RMSD

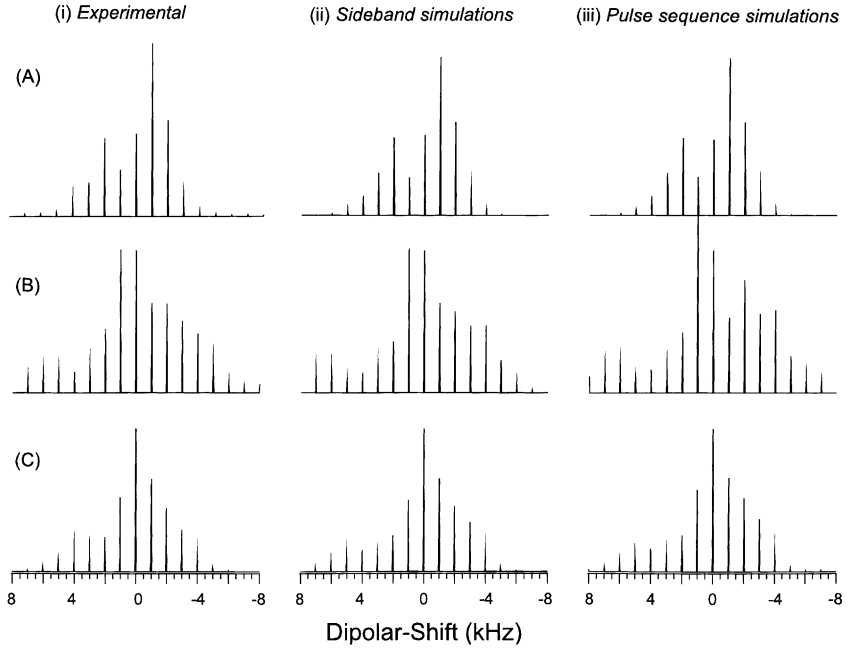

Fig. 6. The one-dimensional dipolar-shift spinning sideband patterns of a powder sample of *N*-acetyl-^{15}N-L-valyl-^{15}N-L-leucine (NAVL) obtained at 4 kHz MAS for the leucine residue. The experimental dipolar-shift spectra obtained from the ω_1 frequency dimension of the 2D spectra (not shown) are shown in column (i). The best fitting simulated spectra are shown in column (ii). The spectra obtained from numerical pulse sequence simulations using the SIMPSON program are shown in column (iii). (A) Spinning sideband patterns of ^{15}N CSA; (B) spinning sideband patterns of dipolar-shift interactions with two rotor periods of dipolar coupling evolution; (C) spinning sideband patterns of dipolar-shift interactions with one rotor period of dipolar coupling evolution. The simulated spectra were obtained using ^{15}N CSA principal values of $\sigma_{11N} = 56.6$ ppm, $\sigma_{22N} = 102.9$ ppm, $\sigma_{33N} = 225.4$ ppm. The (α_N, β_N) angles used in simulated dipolar-shiftspectra were ($48 \pm 15°$, $16 \pm 2°$) in (B) and ($36 \pm 20°$, $15 \pm 2°$) in (C). An N–H bond length of 1.06 Å and a spinning speed of 1 kHz were used in the simulations.

values were calculated by varying α_N from 0° to 90° and β_N from 10° to 30°. The resulting contour plots are shown in Figs. 5A and C for 4- and 2-kHz spectra, respectively. The contour levels are normalized relative to the minimum RMSD value, which was set to 1. The contour interval was 0.1 of the minimum RMSD value and the errors for the α_N and β_N angles were estimated at 1.1 contour level. The numerically simulated spectra are shown in Figs. 3B-iii and 4B-iii using the same parameters as described before, except that LG decoupling was used in both the rotor periods of the t_1 period.

Figs. 3C-i and 4C-i show the spectra obtained with LG decoupling in the first rotor period and CW decoupling in the second rotor period. Therefore, the CSA interaction is fully effective, while the heteronuclear dipolar coupling is effective only in the first rotor period of t_1. Thus the dipolar coupling is reduced by half in addition to the scaling factor from the LG decoupling. The best-fit spectra in Figs. 3C-ii and 4C-ii were obtained using the same CSA principal values as given above, but half of the dipolar coupling. The angles (α_N, β_N) used in the best-fit spectra are (36°, 16°) in Fig. 3C-ii and (32°, 18°) in Fig. 4C-ii, which are also listed in Table 1. The RMSD contour plots are shown in Figs. 5B and D. The spectra shown in Figs. 3C-iii and 4C-iii were obtained by simulating the pulse sequence numerically, setting the first rotor period with LG decoupling and the second rotor period with CW decoupling of protons.

The same analyses were also performed on the NAVL sample. The one-dimensional dipolar-shift spectral slices obtained from the 2D spectra under 4 kHz MAS are given in Figs. 6 and 7 for leucine and valine residues, respectively. The (α_N, β_N) angle pairs used for the full dipolar-shift best-fit spectra are (48°, 16°) for the leucine residue and (54°, 17°) for the valine residue (Table 1). For partial dipolar-shift spectra, the (α_N, β_N) angle pairs were optimized at (36°, 15°) for the leucine residue and (27°, 16°) for the valine residue (Table 1). An N–H bond length of 1.06 Å was used in all simulations. The α_N and β_N angles obtained from the present study within experimental errors are in good agreement with the values measured using a two-dimensional MADMAT (magic angle decoupling magic angle turning) experiment on the same sample [8].

Two-dimensional experiments were also performed at 8 kHz MAS and four rotor periods on a $^{13}C_\alpha$-labeled L-leucine sample to examine the efficacy of the proposed method. From the crystal structure of L-leucine, two asymmetric molecules are present in a unit cell [29], and two $^{13}C_\alpha$ peaks, therefore, appear in the 1D spectrum with the isotropic chemical shifts at 54.4 (site 1) and 53.4 ppm (site 2). Fig. 8 shows the 1D spectral slices for both these sites (2D spectra not shown). Simulations of the CSA

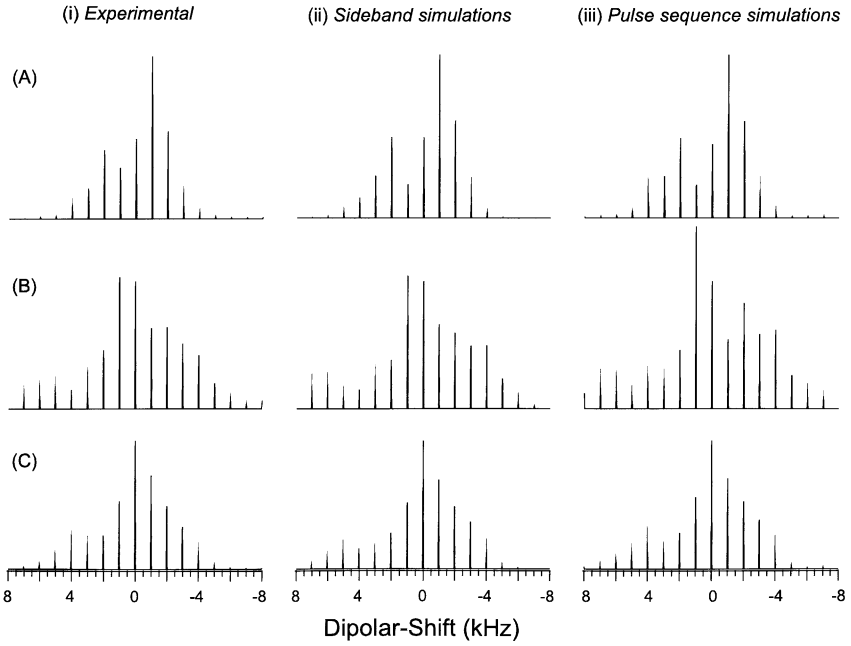

Fig. 7. The one-dimensional dipolar-shift spinning sideband patterns of a powder sample of *N*-acetyl-^{15}N-L-valyl–^{15}N-L-leucine (NAVL) obtained at 4 kHz MAS for the valine residue. The experimental dipolar-shift spectra obtained from the ω_1 frequency dimension of the 2D spectra (not shown) are shown in column (i). The best fitting simulated spectra are shown in column (ii). The spectra obtained from numerical pulse sequence simulations using the SIMPSON program are shown in column (iii). (A) Spinning sideband patterns of ^{15}N CSA; (B) spinning sideband patterns of dipolar-shift interactions with two rotor periods of dipolar coupling evolution; (C) spinning sideband patterns of dipolar-shift interactions with one rotor period of dipolar coupling evolution. The simulated spectra were obtained using the ^{15}N CSA principal values of $\sigma_{11N} = 57.3$ ppm, $\sigma_{22N} = 93.9$ ppm, $\sigma_{33N} = 226.5$ ppm. The (α_N, β_N) angles used in simulated dipolar-shift spectra were ($54 \pm 20°$, $17 \pm 2°$) in (B) and ($27 \pm 25°$, $16 \pm 2°$) in (C). An N–H bond length of 1.06 Å and a spinning speed of 1 kHz were used in the simulations.

patterns for both the sites (Figs. 8A and C) yielded the principal values of $\sigma_{11C} = 43.8$, $\sigma_{22C} = 56.1$, and $\sigma_{33C} = 63.3$ ppm for the site 1 and $\sigma_{11C} = 43.0$, $\sigma_{22C} = 55.4$, and $\sigma_{33C} = 61.9$ ppm for the site 2 (Table 1). The span of the magnitude of the CSA tensor of the C_α carbon (2 kHz) is significantly smaller than that of the ^{13}C–^{1}H dipolar coupling (20.4 kHz for a C–H bond length of 1.14 Å). Therefore, reducing the magnitude of the ^{13}C–^{1}H dipolar coupling was essential to obtain an interpretable dipolar-shift spectrum in order to determine the $^{13}C_\alpha$ CSA tensor in the molecular frame. The application of the LG decoupling during part of the t_1 evolution period can significantly reduce the magnitude of the ^{13}C–^{1}H dipolar coupling. The spectra in Figs. 8B and D were obtained with one rotor period of LG decoupling and three rotor periods of CW decoupling of protons, respectively. Therefore, the residual dipolar coupling is only one-fourth of the original magnitude. Simulations of the spinning sidebands were performed using a dipolar coupling of 5.1 kHz and (α_N, β_N) angle pairs of (0°, 90°) for both the C_α sites. Both experiments and numerical pulse sequence simulations demonstrated the successful performance of the partial LG decoupling in reducing the effective heteronuclear dipolar coupling by 0.25.

To our knowledge, only a few C_α CSA tensors have been determined experimentally to a high accuracy. The previously reported L-leucine C_α tensor values are very different from our data (Table 1), and this is because the previous data were obtained from slow spinning one-dimensional CPMAS experiments on natural abundance samples, and the tensor values were extracted from very crowded spectra [30]. Our data were obtained using a ^{13}C-labeled sample and 2D separation experiments, and the spectra are clear of overlaps with other carbon spins, resulting in a much higher accuracy. The L-leucine C_α tensor values determined here are in a comparable range with those obtained from L-alanine [31] and L-threonine [32] single crystals (Table 1) and ab initio calculations for several amino acids [3].

5. Sources of experimental error

It is important to develop simple pulse sequences that can be used to measure the complete CSA tensors (both the magnitudes and the orientations of the principal elements) directly from proteins for structural studies using NMR spectroscopy. This is technically demanding, especially in the case of proteins or peptides embedded in hydrated lipid bilayers, where the calibration of rf pulse width or power is usually performed on test samples. This experimental set-up procedure may not be correct and may lead to pulse imperfections. Therefore, it is useful to analyze the effects of experimental

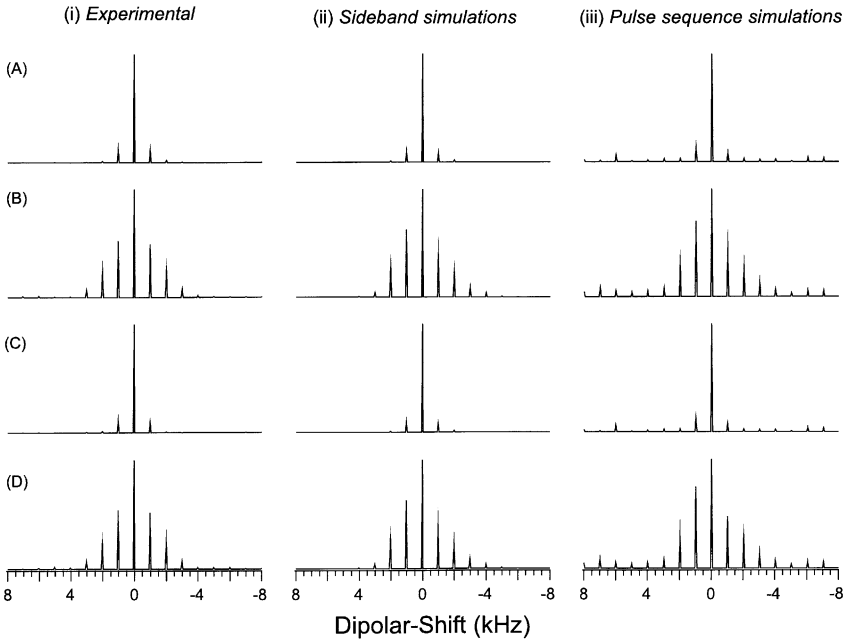

Fig. 8. The one-dimensional dipolar-shift spinning sideband patterns of a powder sample of $^{13}C_{\alpha}$-L-leucine obtained at 8 kHz MAS using four rotor periods of t_1 evolution time (one rotor period of LG and three rotor periods of CW decoupling). The experimental dipolar-shift spectra obtained from the ω_1 frequency dimension of the 2D spectra (not shown) are shown in column (i). The best fitting simulated spectra are shown in column (ii). The spectra obtained from numerical pulse sequence simulations using the SIMPSON program are shown in column (iii). (A) Spinning sideband patterns of the $^{13}C_{\alpha}$ CSA for site 1 with isotropic shift of 54.4 ppm; (B) spinning sideband patterns of dipolar-shift interactions for site 1 with one rotor period of dipolar coupling evolution; (C) spinning sideband patterns of the $^{13}C_{\alpha}$ CSA for site 2 with isotropic shift of 53.4 ppm; (D) spinning sideband patterns of dipolar-shift interactions for site 2 with one rotor period of dipolar coupling evolution. The simulated spectra were obtained using the $^{13}C_{\alpha}$ CSA principal values of $\sigma_{11C} = 43.8$ ppm, $\sigma_{22C} = 56.1$ ppm, $\sigma_{33C} = 63.3$ ppm for site 1 and $\sigma_{11C} = 43.0$ ppm, $\sigma_{22C} = 55.4$ ppm, $\sigma_{33C} = 61.9$ ppm for site 2. The (α_N, β_N) angles used in simulated dipolar-shift spectra were $(0 \pm 20°, 90 \pm 5°)$ in (B) and (D). A C–H bond length of 1.14 Å and a spinning speed of 1 kHz were used in the simulations.

imperfections on the efficacy of the proposed two-dimensional pulse sequences. Numerical simulations of the performance of the pulse sequences were carried out using the SIMPSON program. The CSA and dipolar parameters for the NAV sample, a two-rotor period evolution time, and a 4-kHz spinning speed were used in the simulations. Pulse imperfections such as errors in the π pulse length or the rf field inhomogeneity and the resonance offset are considered. Numerically simulated one-dimensional spinning sideband patterns for CSA, CSA + full ^1H–^{15}N dipolar coupling, and CSA + partial ^1H–^{15}N dipolar coupling obtained using the pulse sequences in Figs. 1B and C, respectively, are compared with perfect spectra (obtained without any pulse errors). Fig. 9 shows the RMSD plot that represents the difference between spectra obtained with an imperfect π pulse and the perfect spectrum against the rf field inhomogeneity (Fig. 9A) and resonance offset (Fig. 9B). It is obvious from Figs. 9A and B that the spinning sideband patterns are highly dependent on the quality of the π pulse employed in pulse sequences. Therefore, care must be taken to calibrate the π pulse before setting up the experiment for the measurement of CSA tensors using these two-dimensional pulse sequences. It should be noted that the errors are larger when the magnitude of the heteronuclear interaction is larger (see Figs. 9A and B). Therefore, scaling down the heteronuclear dipolar interaction using a partial LG decoupling strategy as shown in Fig. 1C should be highly useful to measure CSA tensors from biological samples, particularly to study membrane-associated proteins embedded in hydrated lipid bilayers.

One of the major disadvantages of these 2D experiments is that it has to be performed on resonance. If the rf carrier frequency is higher than the isotropic chemical shift then the intensities of the sidebands with a positive order increase and those of sidebands with a negative order decrease (simulations not shown). On the other hand, if the rf carrier frequency is lower than the isotropic chemical shift then the intensities of those sidebands with a negative order increase and those of sidebands with a positive order decrease (simulations not shown). This trend holds true for all CSA and dipolar-shift experiments. From the RMSD values, the isotropic off-resonance up to ± 1 ppm is acceptable. Nevertheless, it may be possible to overcome the off-resonance problems using procedures presented elsewhere [11]. No such efforts were made in this study.

One more possible source of experimental errors in the measurement of CSA tensors using these 2D tech-

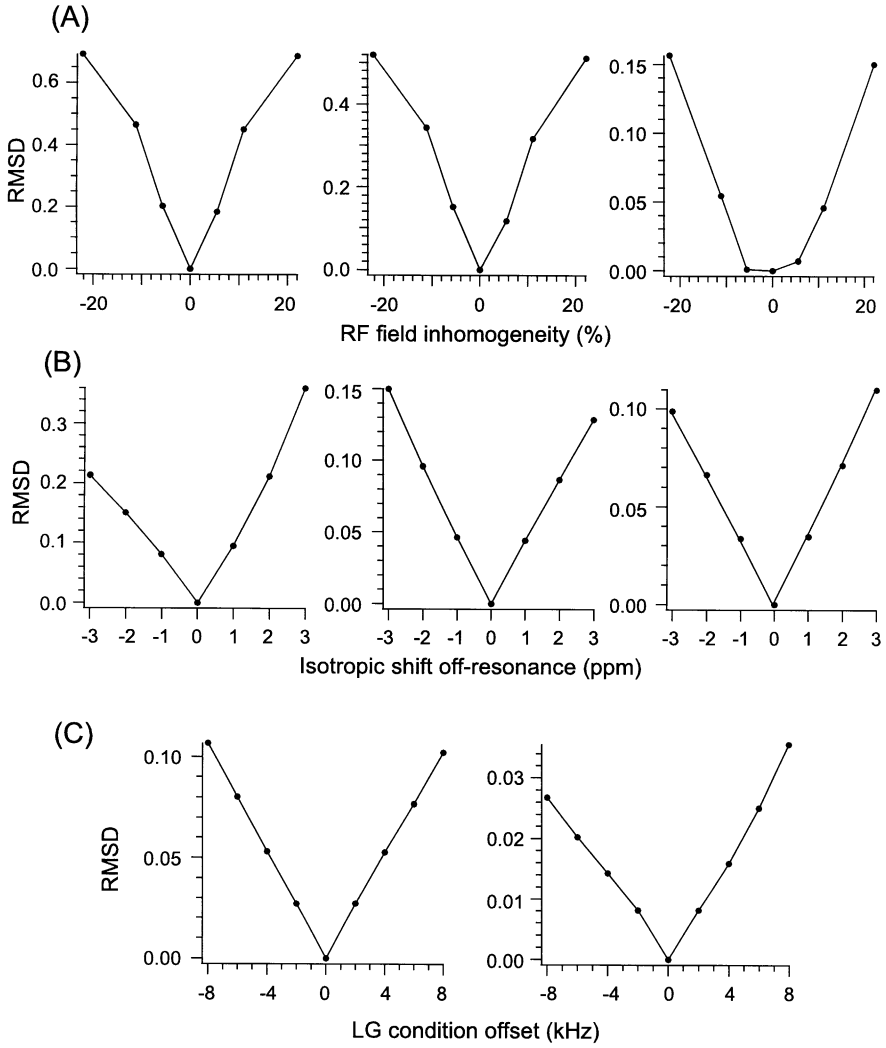

Fig. 9. The efficacy of the pulse sequences given in Fig. 1 against the effects of the X-channel π pulse length errors (A) and offset (B) and an error in the offset value during the LG decoupling (C), illustrated by numerical simulations using the SIMPSON program. The CSA and dipolar coupling parameters of the NAV sample were used in the simulations. A two-rotor-period experiment with a spinning speed of 4 kHz is considered. Spectra displayed in the leftmost columns of (A) and (B) were obtained using CW decoupling for both t_1 evolution rotor periods. Spectra displayed in the middle columns of (A) and (B), and the left plot of (C) were obtained using LG decoupling for both t_1 evolution rotor periods. Spectra displayed in the rightmost columns of (A), (B), and (C) were obtained using LG decoupling for the first rotor period and CW decoupling for the second rotor period of evolution. (A) The π pulse length on the ^{15}N rf channel was offset by 0, ±0.5, ±1.0, and ±2.0 μs from the correct value. The RMSD values for the π pulse imperfection were calculated by comparing with the spectrum that was obtained using a perfect π pulse, and plotted against the percentage of the offset. (B) The ^{15}N isotropic shifts were set to be 0, ±1, ±2, and ±3 ppm from the rf carrier frequency. The RMSD values for off-resonance effects were calculated by comparing with the spectrum that was obtained with the isotropic chemical shift at on-resonance and plotted against the value of off-resonance. (C) The ^{1}H decoupling frequency offsets were 0, ±2, ±4, ±6, and ±8 kHz from the perfect LG condition. Left: LG decoupling for both evolution rotor periods; right: LG decoupling for the first rotor period and CW decoupling for the second rotor period of evolution. The RMSD values for LG offset were calculated by comparing with the spectrum that was obtained with a perfect LG condition and plotted against the LG offset.

niques is the error in setting up the LG condition [19]. The LG condition is experimentally set up using the magnitude (B_{rf}) and carrier frequency (B_{off}) of the rf decoupling power used to decouple protons in the t_1 period of the pulse sequences in Figs. 1B and C. The value of B_{off} is chosen based on the experimental measurement of the B_{rf} value. As mentioned above, B_{rf} is typically measured on a test sample and it may not be correct for a relevant protein sample. This could be a possible source of experimental error (the value of B_{rf} or B_{off}) in the measurement of CSA tensors. Numerical simulations of the performance of the pulse sequences in Fig. 1 were performed using the CSA tensors of the NAV sample. In the numerical simulations, we deliberately offset the value of B_{off} from the perfect LG condition by ±2, ±4, ±6, and ±8 kHz, and the RMSD errors against B_{off} are shown in Fig. 9C for two rotor periods of LG (left) and one rotor period of LG (right).

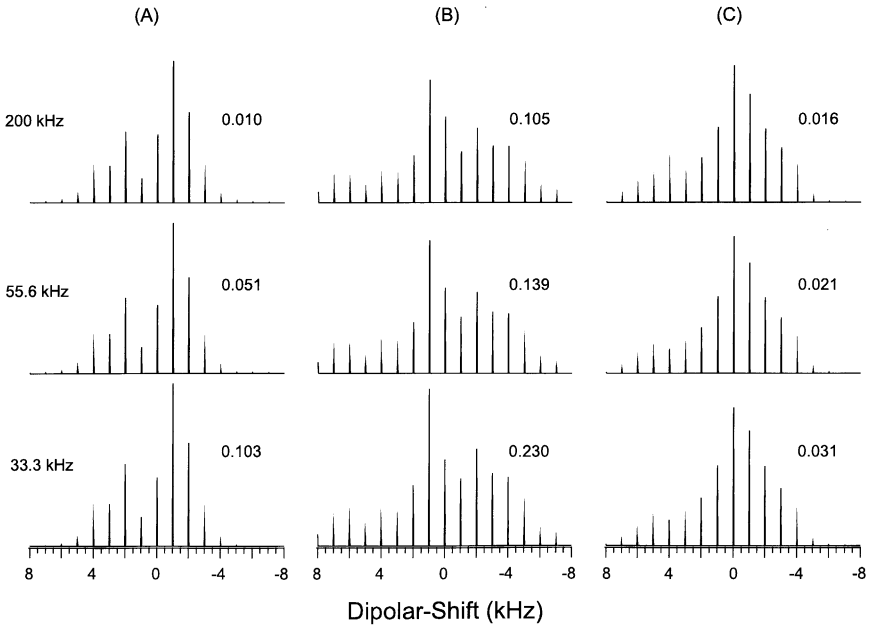

Fig. 10. Numerical simulations of the effects of errors in the rf power level used for the π pulse on the X-channel on the amplification and recovery of the dipolar-shift interactions using the pulse sequences given in Fig. 1. The CSA and dipolar coupling parameters of the NAV sample were used in simulations of two-rotor-period experiments with a spinning speed of 4 kHz. The rf power level was set to 200, 55.6, and 33.3 kHz on ^{15}N. (A) CW decoupling for both evolution rotor periods; (B) LG decoupling for both evolution rotor periods; (C) LG decoupling for the first rotor period and CW decoupling for the second rotor period of evolution. The number next to each spectrum is the RMSD value from the direct sideband simulation (see Fig. 3, column ii).

Although a deviation from the perfect LG condition introduces a slightly larger RMSD value due to a change in the scaling factor of the LG sequence from 0.58, the effect is reasonably small for B_{off} errors < 5 kHz (see Fig. 9C). Inclusion of more protons in addition to the amide proton and the long-range ^{1}H–^{1}H dipolar interactions from additional protons did not cause a significant change in the simulated results.

It is also important to examine the performance of the 2D pulse sequence against the rf power of the π pulse as most of the biological samples, especially the wet samples, are power lossy and it is practically difficult to use high-power pulses. Spectra simulated using the SIMPSON program for various π pulse powers, (200, 55.6, and 33.3 kHz) are given in Fig. 10. The RMSD values listed in Fig. 10 are obtained by comparing the corresponding numerically simulated spectrum and the spectrum obtained from the direct sideband simulation using the CSA tensor parameters of NAV sample (see Fig. 3, column ii). Although higher power levels resulted in better spectra (smaller RMSD), we found that the performance of the 2D pulse sequences at lower rf power levels (for example ~ 50 kHz) is reasonably good (see Fig. 10).

6. Conclusions

The present work explored the possibility of employing 2D pulse sequences that amplify inhomogeneous interactions, such as the CSA and heteronuclear dipolar interactions, under MAS to determine CSA tensors from multiple sites. Such efforts represent an attempt to exploit ongoing development of multidimensional pulse sequences for CSA tensor measurements from a uniformly labeled protein which hitherto demanded the use of samples labeled with X (^{15}N or ^{13}C) isotope at a single site. Pursuing such an avenue may not only simplify the execution and analysis of NMR experiments but also, by lifting the demand for either no or slow spinning conditions, open up the sensitivity and resolution bonuses that result from high-field fast MAS operation.

The closeness of a spinning sideband pattern (either CSA or dipolar-shift) obtained using a 2D pulse sequence in this work to the 1D spectrum directly obtained by the conventional CPMAS experiment suggests that the 2D methods are highly efficient in resolving the amplified inhomogeneous interactions associated with the chemically and/or magnetically inequivalent X (^{15}N or ^{13}C) nuclei sites in a polypeptide labeled uniformly with the X isotope. Further, the feasibility of obtaining the CSA and the dipolar coupling tensors with a fast spinning speed (up to 10 kHz) using the 2D methods demonstrated in this study suggests that these methods are also highly sensitive as compared to other slow spinning techniques. In these experiments, the total number of spinning sidebands is greatly enhanced due to the amplification of the magnitude of an inhomogeneous

interaction or due to an effective reduction of the spinning speed to $\omega_r/2n$. The use of the LG sequence for the partial decoupling of ^1H–^1H dipolar interactions greatly enhances the flexibility of the method by effectively reducing the dipolar to CSA ratio.

Acknowledgments

This research was supported by the NSF through Grant MCB-9875756 (CAREER Award).

References

[1] R.Q. Fu, T.A. Cross, Solid-state nuclear magnetic resonance investigation of protein and polypeptide structure, Annu. Rev. Biophys. Biomol. Struct. 28 (1999) 235–268.
[2] D.K. Lee, R.J. Wittebort, A. Ramamoorthy, Characterization of N-15 chemical shift and H-1–N-15 dipolar coupling interactions in a peptide bond of uniaxially oriented and polycrystalline samples by one-dimensional dipolar chemical shift solid-state NMR spectroscopy, J. Am. Chem. Soc. 120 (1998) 8868–8874.
[3] R.H. Havlin, H.B. Le, D.D. Laws, A.C. deDios, E. Oldfield, An ab initio quantum chemical investigation of carbon-13 NMR shielding tensors in glycine, alanine, valine, isoleucine, serine, and threonine: comparisons between helical and sheet tensors and the effects of (chi)(1) on shielding, J. Am. Chem. Soc. 119 (1997) 11951–11958.
[4] A.E. Walling, R.E. Pargas, A.C. deDios, Chemical shift tensors in peptides: a quantum mechanical study, J. Phys. Chem. A 101 (1997) 7299–7303.
[5] D.K. Lee, J.S. Santos, A. Ramamoorthy, Application of one-dimensional dipolar shift solid-state NMR spectroscopy to study the backbone conformation of membrane-associated peptides in phospholipid bilayers, J. Phys. Chem. B 103 (1999) 8383–8390.
[6] C. Scheurer, N.R. Skrynnikov, S.F. Lienin, S.K. Straus, R. Bruschweiler, R.R. Ernst, Effects of dynamics and environment on N-15 chemical shielding anisotropy in proteins: a combination of density functional theory, molecular dynamics simulation, and NMR relaxation, J. Am. Chem. Soc. 121 (1999) 4242–4251.
[7] M. Hong, Solid-state NMR determination of C-13 alpha chemical shift anisotropies for the identification of protein secondary structure, J. Am. Chem. Soc. 122 (2000) 3762–3770.
[8] D.K. Lee, Y.F. Wei, A. Ramamoorthy, A two-dimensional magic-angle decoupling and magic-angle turning solid-state NMR method: an application to study chemical shift tensors from peptides that are nonselectively labeled with N-15 isotope, J. Phys. Chem. B 105 (2001) 4752–4762.
[9] D.P. Raleigh, M.H. Levitt, R.G. Griffin, Rotational resonance in solid-state NMR, Chem. Phys. Lett. 146 (1988) 71–76.
[10] Y.F. Wei, D.K. Lee, A. Ramamoorthy, Solid-state C-13 NMR chemical shift anisotropy tensors of polypeptides, J. Am. Chem. Soc. 123 (2001) 6118–6126.
[11] T. Gullion, Extended chemical-shift modulation, J. Magn. Reson. 85 (1989) 614–619.
[12] M. Hong, J.D. Gross, C.M. Rienstra, R.G. Griffin, K.K. Kumashiro, K. Schmidt-Rohr, Coupling amplification in 2D MAS NMR and its application to torsion angle determination in peptides, J. Magn. Reson. 129 (1997) 85–92.
[13] M. Hong, R.G. Griffin, Resonance assignments for solid peptides by dipolar-mediated C-13/N-15 correlation solid-state NMR, J. Am. Chem. Soc. 120 (1998) 7113–7114.
[14] S.M. de Paul, K. Saalwachter, R. Graf, H.W. Spiess, Sideband patterns from rotor-encoded longitudinal magnetization in MAS recoupling experiments, J. Magn. Reson. 146 (2000) 140–196.
[15] M. Carravetta, M. Eden, X. Zhao, A. Brinkmann, M.H. Levitt, Symmetry principles for the design of radiofrequency pulse sequences in the nuclear magnetic resonance of rotating solids, Chem. Phys. Lett. 321 (2000) 205–215.
[16] A. Brinkmann, M.H. Levitt, Symmetry principles in the nuclear magnetic resonance of spinning solids: heteronuclear recoupling by generalized Hartmann–Hahn sequences, J. Chem. Phys. 115 (2001) 357–384.
[17] X. Zhao, M. Eden, M.H. Levitt, Recoupling of heteronuclear dipolar interactions in solid-state NMR using symmetry-based pulse sequences, Chem. Phys. Lett. 342 (2001) 353–361.
[18] S. Hafner, H.W. Spiess, Advanced solid state NMR spectroscopy of strongly dipolar coupled spins under fast magic angle spinning, Concepts Magn. Reson. 10 (1998) 99–128.
[19] M. Lee, W.I. Goldburg, Nuclear magnetic resonance line narrowing by a rotating rf field, Phys. Rev. A 140 (1965) 1261–1271.
[20] A. Bielecki, A.C. Kolbert, H.J.M. DE Groot, R.G. Griffin, M.H. Levitt, Frequency-switched Lee–Goldberg sequences in solids, Adv. Magn. Reson. 14 (1990) 111–124.
[21] D.K. Lee, A. Ramamoorthy, A simple one-dimensional solid-state NMR method to characterize the nuclear spin interaction tensors associated with the peptide bond, J. Magn. Reson. 133 (1998) 204–206.
[22] A.E. Bennett, C.M. Rienstra, M. Auger, K.V. Lakshmi, R.G. Griffin, Heteronuclear decoupling in rotating solids, J. Chem. Phys. 103 (1995) 6951–6958.
[23] K. Takegoshi, T. Terao, C-13–H-1 dipolar recoupling under very fast magic-angle spinning using virtual pulses, Solid State Nucl. Magn. Reson. 13 (1999) 203–212.
[24] K. Takegoshi, T. Imaizumi, T. Terao, One- and two-dimensional C-13–H-1/N-15–H-1 dipolar correlation experiments under fast magic-angle spinning for determining the peptide dihedral angle ϕ, Solid State Nucl. Magn. Reson. 16 (2000) 271–278.
[25] S.A. Smith, T.O. Levante, B.H. Meier, R.R. Ernst, Computer-simulations in magnetic-resonance—an object-oriented programming approach, J. Magn. Reson. Ser. A 106 (1994) 75–105.
[26] M. Bak, J.T. Rasmussen, N.C. Nielsen, SIMPSON: a general simulation program for solid-state NMR spectroscopy, J. Magn. Reson. 147 (2000) 296–330.
[27] J. Herzfeld, A.E. Berger, Sideband intensities in NMR-spectra of samples spinning at the magic angle, J. Chem. Phys. 73 (1980) 6021–6030.
[28] H.J.M. de Groot, S.O. Smith, A.C. Kolbert, J.M.L. Courtin, C. Winkel, J. Lugtenburg, J. Herzfeld, R.G. Griffin, Iterative fitting of magic-angle-spinning NMR-spectra, J. Magn. Reson. 91 (1991) 30–38.
[29] M. Coll, X. Solans, M. Font-Altaba, J.A. Subirana, Structure of L-leucine—a redetermination, Acta Crystallogr. Sect. C Cryst. Struct. Commun. 42 (1986) 599–601.
[30] C.H. Ye, R.Q. Fu, J.Z. Hu, L. Hou, S.W. Ding, C-13 Chemical-shift anisotropies of solid amino-acids, Magn. Reson. Chem. 31 (1993) 699–704.
[31] A. Naito, S. Ganapathy, K. Akasaka, C.A. McDowell, Chemical shielding tensor and C-13–N-14 dipolar splitting in single-crystals of L-alanine, J. Chem. Phys. 74 (1981) 3190–3197.
[32] N. Janes, S. Ganapathy, E. Oldfield, C-13 chemical shielding tensors in L-threonine, J. Magn. Reson. 54 (1983) 111–121.